AN ANN CORRELATION OF LIFT COEFFICIENTS OF BUBBLES IN LINEAR SHEAR FLOWS

Hayashi, Kosuke
Chen, Junming
Kurimoto, Ryo
Tomiyama, Akio

(Citation)
Multiphase Science and Technology,34(2):67-82

(Issue Date)
2022

(Resource Type)
journal article

(Version)
Accepted Manuscript

AN ANN CORRELATION OF LIFT COEFFICIENTS OF BUBBLES IN LINEAR SHEAR FLOWS

K. Hayashi,[1,] J. Chen,[1] R. Kurimoto,[1] & A. Tomiyama[1]*

[1]*Graduate School of Engineering, Kobe University, 1-1 Rokkodai, Nada, Kobe, 657-8501, Japan*

*Address all correspondence to: K. Hayashi, Graduate School of Engineering, Kobe University, 1-1 Rokkodai, Nada, Kobe, 657-8501, Japan,
E-mail: hayashi@mech.kobe-u.ac.jp

Original Manuscript Submitted: mm/dd/yyyy; Final Draft Received: mm/dd/yyyy

An artificial neural network (ANN) correlation of the lift coefficients of spherical and deformed bubbles in liner shear flows is developed. The ANN has three hidden layers and the number of neurons in each hidden layer is 10. Lift coefficient data available in literature are used to train and test the ANN correlation. The data include bubbles in both viscous force dominant and surface tension-inertial force dominant regimes. Good agreements between the training data and model predictions are obtained. Comparing the model with the test data confirms that the correlation has a good generalization performance.

KEY WORDS: *lift force, artificial neural network, machine learning*

1. INTRODUCTION

Machine learning has been utilized in a wide variety of scientific fields. In the multiphase flow community, machine learning techniques, especially the artificial neural network (ANN) (Beale and Jackson, 1990), have been applied to multiphase flow researches have been developed, e.g. flow pattern identification from video images (Liu and Bai, 2019; Shibata et al., 2021), subgrid-scale modeling of interfacial mass transfer in DNS of bubbles (Weiner et al., 2019), modeling of heat transfer coefficients (Enoki et al., 2017), predictions of void fractions in upward bubbly flows (Tanaka et al., 2022) and modeling of hydrodynamics in bubble column reactors (Behkish, 2004; Behkish et al., 2005; Tanaka, 2010; Tanaka et al., 2010).

Behkish (2004) developed an ANN for predicting the total gas holdup and the gas holdup of large bubbles in bubble column and slurry bubble column reactors (Behkish et al., 2005). The ANN has two hidden layers in addition to the input and output layers and the neurons are fully-connected. They used over 3,880 and 1,425 data of gas holdups and showed that the trained ANNs predict the training and non-training data with 16% and 10% absolute errors for the former and the latter. Tanaka et al. (2010) also developed ANNs to predict the gas holdup, the dispersion coefficient and the reaction rate, which were used in constitutive equations to close the averaging models for bubble column reactors (Tanaka, 2010). An example of applications of ANN to a two-phase thermal engineering is found in Enoki et al. (2017), in which heat transfer coefficients in horizontal mini-tubes are predicted using an ANN. The ANN consists of the input and output layers and three hidden layers, and the inputs (features) are 16 parameters for the

0276–1459/20/$35.00

physical property and 5 parameters for the flow condition. The ANN trained with over 1,000 heat transfer data was confirmed to give good predictions.

As for the bubble dynamics, an ANN correlation is expected to give good evaluations of model coefficients in the constitutive equations such as the drag, lift and so on, which are required in bubbly flow simulations based on the averaging models. An advantage of the ANN correlation is that it can be easily improved by a re-learning process when new experimental, numerical and analytical data of the model coefficients are available. The key for realizing a reliable and widely-applicable ANN correlation is to accumulate a large number of data, the so-called big data. One of the difficulties in developing an accurate ANN correlation of the lift coefficient is lack of experimental database. However, it would be worth examining the capability of ANN for predicting the lift coefficients even with the limited number of the data.

This study aims to clarify the capability of an ANN correlation to express the lift coefficients of spherical and deformed bubbles in linear shear flows.

2. ARTIFICIAL NEURAL NETWORK

2.1 Structure of ANN

The ANN used in this study consists of the input layer with N inputs, $\mathbf{x}(= (x_1, x_2, \cdots, x_N))$, the Affine layers having the weight matrix $\mathbf{W}$ and the bias $\mathbf{b}$, the batch-normalization (BatchNorm) layer (Ioffe and Szegedy, 2015), the leaky ReLU (Leaky Rectified Linear Unit) layer (Maas et al., 2013) and the identity layer for the output (Figs 1 and 2). All the layers are fully-connected. The $\mathbf{x}$ is weighted and biased by using $\mathbf{W}$ and $\mathbf{b}$ to transform it into the signal, $\mathbf{a}$, and then, is transferred to the neurons in the first hidden layer:

$$a_i = x_j W_{ji} + b_i \tag{1}$$

where W_{ji} are the component of the weight matrix connecting the jth input and the ith neuron in the hidden layer, and b_i is the ith component of $\mathbf{b}$. BatchNorm is applied to the signal $\mathbf{a}$ as

$$\bar{a}_i = \frac{a_i - \mu_{Bi}}{\sigma_{Bi}} \tag{2}$$

where μ_B and σ_B are the mean and the standard deviation of a in the batch. The $\bar{a}$ is scaled by the trainable coefficients, γ and β, as

$$\hat{a}_i = \gamma_i \bar{a}_i + \beta_i \tag{3}$$

The leaky ReLU is then applied to $\hat{\mathbf{a}}$:

$$y_i = \begin{cases} \hat{a}_i & \text{for } \hat{a}_i \geq 0 \\ \alpha \hat{a}_i & \text{for } \hat{a}_i < 0 \end{cases} \tag{4}$$

where the gradient for negative signals is given by $\alpha = 0.01$. The signal, y, goes to the next hidden layer. The output layer applies the identity function and the output is denoted by z.

The ANN is trained by using the gradient descent learning. The NAG (Nesterov Accelerated Gradient) algorithm (Nesterov, 1983) is used for learning. The weight parameters are initialized using the Gaussian distribution (He et al., 2015). The mean squared error is used as the loss function for evaluating the performance of the ANN.

The machine learning application in this study is developed by using the following packages: Keras (version 2.3.1) using TensorFlow (version 2.0.0) backend and Scikit-Learn (version 0.23.2).

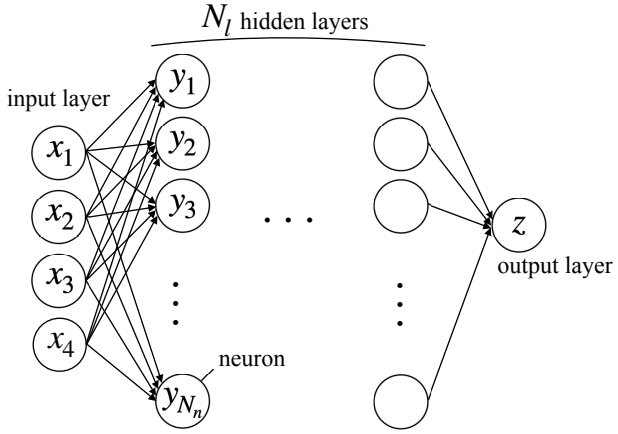

FIG. 1: Fully-connected artificial neural network.

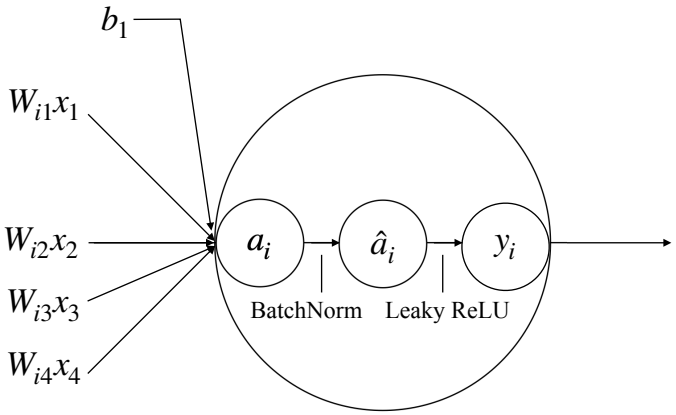

FIG. 2: Signal flow.

2.2 Input and output layers

Multi-fluid models and bubble tracking methods require the lift coefficient C_L when solving the momentum equations. The coefficient depends on several quantities such as the bubble size, the instantaneous bubble and liquid velocities, and the fluid properties, i.e. the gas and liquid densities, the liquid viscosity and the surface tension. It is possible to use these variables as the inputs of the ANN model. However, it would be better to reduce the number of input variables for making the ANN model as simple as possible. For this purpose, the relevant dimensionless groups can be used. The C_L of bubbles in linear shear flows are expected to be expressed in terms of the bubble Reynolds number, Re, the Eötvös number, Eo, and the dimensionless shear rate, Sr (Aoyama et al., 2017; Legendre and Magnaudet, 1998). It has been pointed out that the bubble shape is a key parameter determining the magnitude of the negative component of the lift acting on ellipsoidal bubbles (Adoua et al., 2009; Tomiyama et al., 2002), and the bubble aspect ratio, E, has been taken as one of the independent variables in C_L correlations (Hayashi et al., 2021, 2020; Lee and Lee, 2020; Tomiyama et al., 2002) though E may also be a function of Re, Eo and Sr. Aoyama et al. (2017) pointed out that E is rarely affected by weak liquid shear,

TABLE 1: Dimensionless groups in datasets. A: Aoyama et al. (2017) (clean system), H: Hessenkemper et al. (2021) (purified, deionized, tap), L: Lee and Lee (2020) (contaminated). The values in the parentheses represent the number of data points in each dataset.

	Re	Eo	Sr	M
A (562)	$0.1 \sim 120$	$0.027 \sim 5.0$	$0.03 \sim 0.43$	$2.3 \times 10^{-7} \sim 6.3 \times 10^{-4}$
H (77)	$660 \sim 1520$	$0.68 \sim 5.8$	$0.018 \sim 0.075$	2.6×10^{-11}
L (11)	$440 \sim 7170$	$0.63 \sim 55$	$0.0044 \sim 0.024$	1.4×10^{-11}

and some E correlations are available (Aoyama et al., 2016; Hayashi et al., 2021; Hessenkemper et al., 2021; Ziegenhein et al., 2018). Therefore, Re, Eo, Sr and E are used as the inputs, $\mathbf{x}$, in this study. The C_L is the only output of the present ANN model.

The definitions of the dimensionless groups are as follows:

$$Re = \frac{\rho_L V_R d}{\mu_L} \tag{5}$$

$$Eo = \frac{\Delta\rho g d^2}{\sigma} \tag{6}$$

$$Sr = \frac{\omega d}{V_R} \tag{7}$$

$$E = \frac{d_V}{d_H} \tag{8}$$

where V_R is the bubble relative velocity, d the sphere-volume-equivalent bubble diameter, ρ_L the liquid density, μ_L the liquid viscosity, $\Delta\rho$ is the density difference between the two phases, g the acceleration of gravity, σ the surface tension, ω the velocity gradient of liquid shear flow, d_V and d_H are the minor and major axes of a bubble, and $d = \sqrt[3]{d_V d_H^2}$.

The C_L data were quoted from the literature (Aoyama et al., 2017; Hessenkemper et al., 2021; Lee and Lee, 2020). The numbers of the data points and the ranges of the dimensionless groups are shown in Table 1, where M is the Morton number defined by

$$M = \frac{\mu_L^4 \Delta\rho g}{\rho_L^2 \sigma^3} \tag{9}$$

The Re and Eo range from the order of 10^{-1} to 10^3 and from 0.01 to 10, respectively. The wide ranges of these features may deteriorate the training efficiency. Therefore, $\log Re$ and $\log Eo$ are used instead of Re and Eo to put the data points into narrower variable ranges. Then, all the features are normalized by the mean and the variance of the training data.

The data for training and test are randomly selected from the database with the ratios of 0.8 and 0.2 for the former and the latter, respectively. No stratification is applied in the data extraction. The training data are used in the model development phase, and the test data are used only in the final performance test.

2.3 Numbers of Layers and Neurons

Since the numbers of the input and output neurons are fixed and the network is fully-connected, only parameters of the present ANN model are the number, N_l, of the hidden layer and the number, N_n, of the neurons in the hidden layers. The simplest model examined in the K-folds cross

TABLE 2: Numbers of hidden layers N_l and neurons N_n in each hidden layer.

	$N_l = 1$	2	3	4	5
$N_n = 10$	Case $(1, 10)$	Case $(2, 10)$	Case $(3, 10)$	Case $(4, 10)$	Case $(5, 10)$
20	Case $(1, 20)$	Case $(2, 20)$	Case $(3, 20)$	Case $(4, 20)$	Case $(5, 20)$
30	Case $(1, 30)$	Case $(2, 30)$	Case $(3, 30)$	Case $(4, 30)$	Case $(5, 30)$
40	Case $(1, 40)$	Case $(2, 40)$	Case $(3, 40)$	Case $(4, 40)$	Case $(5, 40)$

TABLE 3: Total numbers of parameters in ANN model. The values in the parentheses are the numbers of non-trainable parameters.

	$N_l = 1$	2	3	4	5
$N_n = 10$	101 (20)	251 (40)	401 (60)	551 (80)	701 (100)
20	201 (40)	701 (80)	1201 (120)	1701 (160)	2201 (200)
30	301 (60)	1351 (120)	2401 (180)	3451 (240)	4501 (300)
40	401 (80)	2201 (160)	4001 (240)	5801 (320)	7601 (400)

validation has $N_l = 1$ and $N_n = 10$. These values are increased up to 5 and 40, respectively, so that the test cases can be summarized as shown in Table 2. For the cases of $N_l > 1$, the same N_n is used for all the hidden layers. The total numbers of the parameters in each ANN model are given in Table 3. Cases $(4, 20)$ and $(2, 40)$ have the same number of neurons. However the total number of the parameters is larger in the latter than in the former.

3. RESULTS AND DISCUSSION

3.1 K-folds Cross Validation

The performances of the ANNs of different N_n and N_l are examined by using the K-folds cross validation. The number of folds is five. The losses in the training L_t and validation L_v are averaged for the folds. 20% of the training set are randomly extracted for validation in each fold. The learning rate and the momentum in NAG are 0.1 and 0.9, respectively. The batch size is set to the size of the training set.

Figure 3 shows the loss histories in each case. In Case $(1, 10)$, the simplest model among the models tested, L_t steeply decreases with increasing the epoch at the early stage of the training. The decreasing rate of L_t then decreases and L_t approaches a certain value (~ 0.006). The L_v also shows a steep reduction at the early stage. However after 400 epochs L_v increases, which implies that the model overfits the training data. The L_v then approaches a certain value, which is about ten times larger than the converged value in the training. The increase in N_l to $N_l = 2$ does not affect L_t so much. On the other hand, the overfitting is mitigated. Using $(N_l, N_n) = (3, 10)$ makes L_t smaller, but the overfitting becomes remarkable. The L_t in Case $(4, 10)$ is smaller than that in $(2, 10)$, whereas L_v in the former is larger.

Compared with Case $(1, 10)$, L_t in Case $(2, 10)$ is smaller and the overfitting is mitigated. By increasing N_n from 10 to 20, L_t is slightly reduced, but further increase in N_n does not affect L_t so much. The L_v in the cases of $N_l = 2$ are similar.

The characteristics of L_t and L_v of $N_l = 3$ and 4 are similar to those of $N_l = 2$. Though Case $(5, 10)$ exhibits a large deterioration of L_v due to overfitting around 5,000 epoch, the other cases of $N_l = 5$ also show trends similar to those in the cases of $N_l = 3$ and 4.

In summary, L_v of $N_l = 1$ are larger than those in the other cases of $N_l > 1$ and the

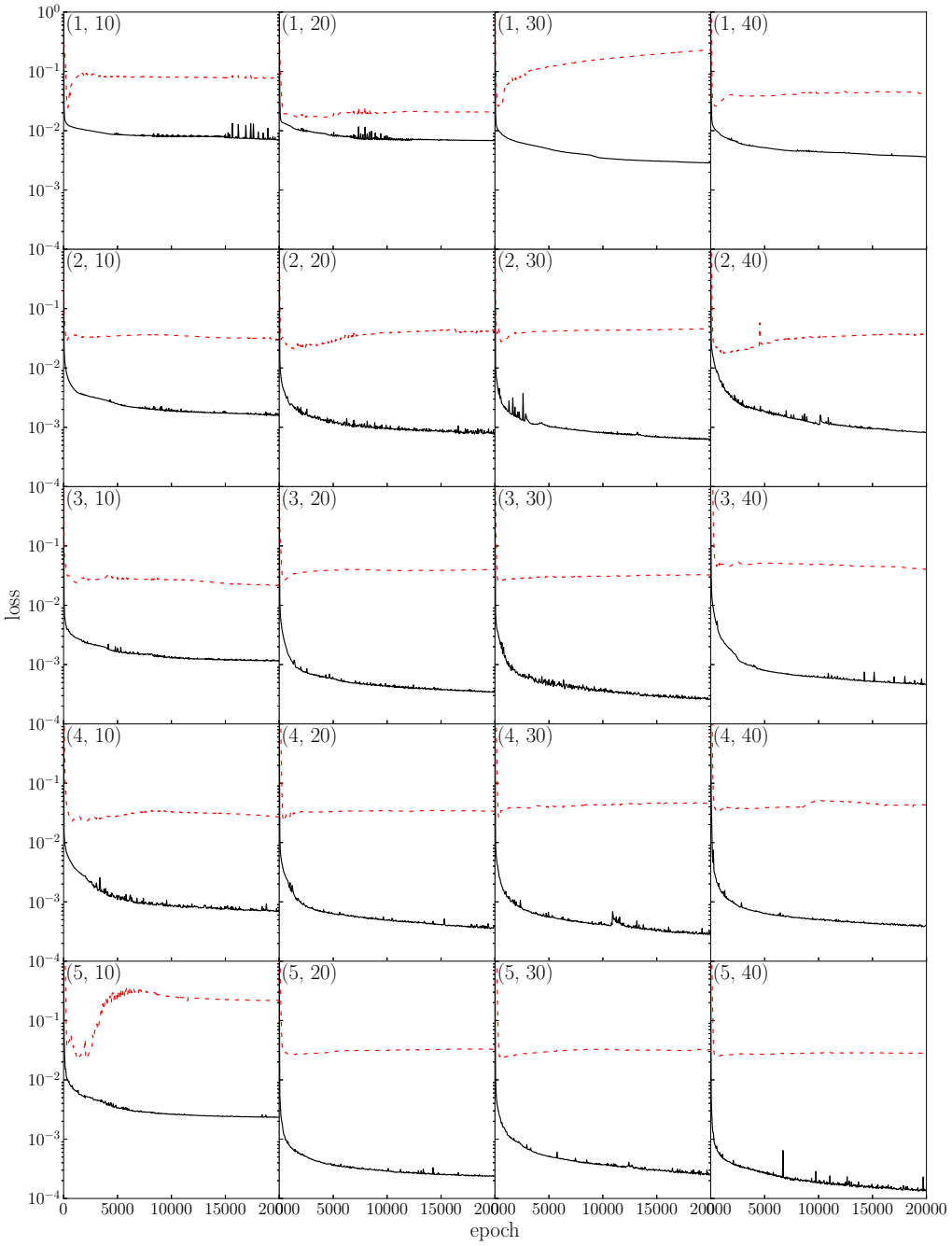

FIG. 3: Loss history in K-folds cross validation in each Case (N_l, N_n). Solid line: loss in training; Dashed line: loss in validation.

overfitting largely deteriorates the performance in some cases. The behaviors of L_v in the cases of $N_l > 1$ seem more stable except for $(5, 10)$. However the increase in N_l from three to larger values are not effective. Although the increase in N_l decreases L_t in most cases, the orders of the magnitude of L_v are not so different. Therefore, $(2, 10)$ or $(3, 10)$ would be a reasonable choice as the base model to make the model as simple as possible. Figure 4 shows the loss histories of these cases up to 50,000 epochs. In both cases, overfitting does not take place even for large epochs. The latter case shows slightly better performance than the former. In the following, we use the model of $(3, 10)$ as the base model.

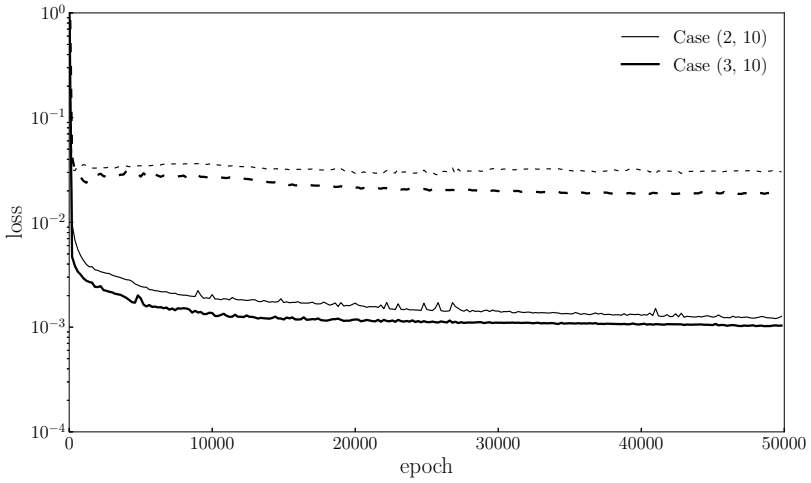

FIG. 4: Comparison of loss history between Cases $(2, 10)$ and $(3, 10)$. Solid line: loss in training; Dashed line: loss in validation.

3.2 Training Phase

The model of $N_n = 3$ and $N_l = 10$ is trained for the full training dataset. Figure 5 shows the loss history in the training phase of the model. The trend of the loss curve is the same as that in the cross validation though the value of L_t of this training is somewhat smaller. Though L_t shows some oscillations possibly due to the large learning rate, the decreasing rate in L_t is very small for epoch $> 20,000$. This implies that the simple model structure $(3, 10)$ does not cause serious overfitting even with the small size of the dataset.

Figure 6 shows comparisons between the predicted C_L (the closed symbols) and the training data (the open symbols), where the model parameters are for 50,000 epochs. The comparisons confirm that the present ANN model is well trained for the dataset for the wide ranges of the relevant dimensionless groups, e.g. $0.1 \leq Re \leq 7000$. Bubbles included in the datasets are either in the viscous force dominant regime or in the surface tension-inertial force dominant regime (Tomiyama et al., 1998), and lift correlations may be developed using different functional forms for those regimes (Hayashi et al., 2021, 2020). On the other hand, the ANN correlation can cover C_L in both regimes with the single network structure. Figure 7 shows the evaluation errors in the predicted C_L, where the dotted lines represent $\pm 10\%$ errors. Most data are within the 10% error range.

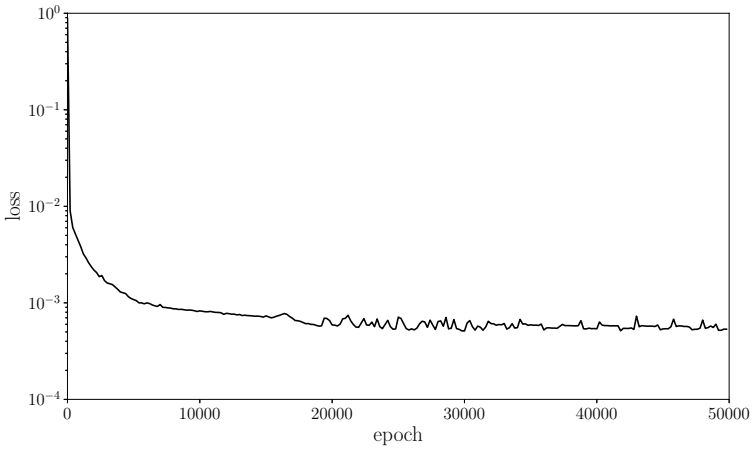

FIG. 5: Loss history in training phase for model of $N_l = 3$ and $N_n = 10$.

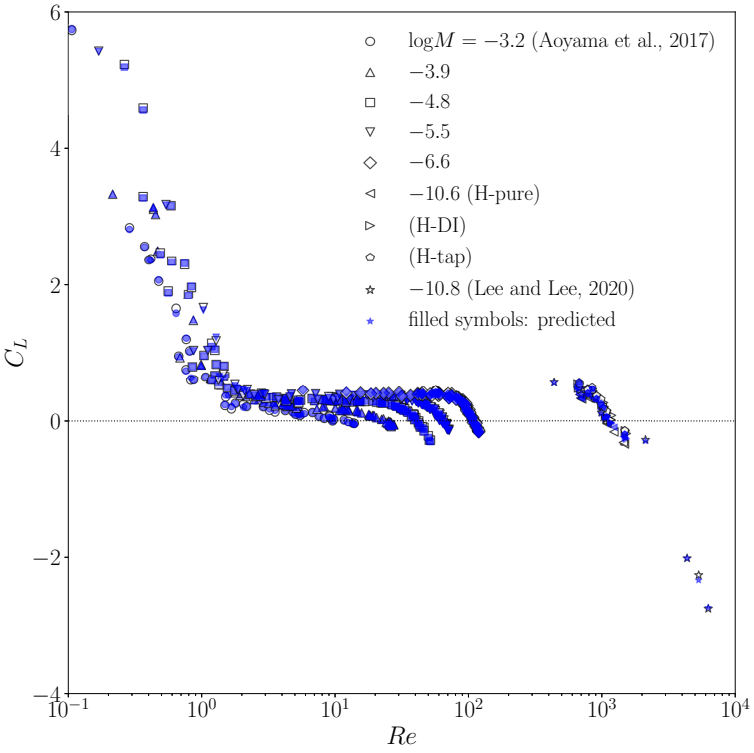

FIG. 6: Comparison between predicted C_L with training data ($N_l = 3$ and $N_n = 10$). Closed symbols: predicted; Open symbols: training data. H-pure, H-DI and H-tap denote bubbles in pure water, deionized water and tap water, respectively (Hessenkemper et al., 2021).

Lift curves are drawn by using the trained ANN as shown in Fig. 8. The inputs were prepared as follows:

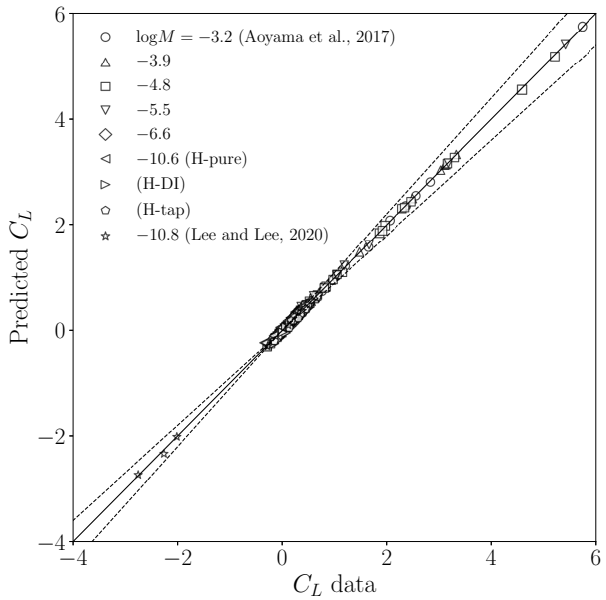

FIG. 7: Estimation errors for training data. $N_l = 3$ and $N_n = 10$.

1. Create data of Re for a certain range.
2. Calculate Eo for the Re data by using the following drag correlations (Chen et al., 2019; Mendelson, 1967; Tomiyama et al., 1998):

$$C_D = \frac{16}{Re}\left[1 + \frac{0.25Re^{0.32}}{E^{1.9}}\right] \quad \text{(viscous force dominant regime)} \tag{10}$$

$$C_D = \frac{8}{3}\frac{Eo}{Eo+4} \quad \text{(surface tension-inertial force dominant regime)} \tag{11}$$

3. Evaluate E by using the following shape correlations (Aoyama et al., 2017; Hayashi et al., 2021):

$$E = (1 + 0.016Eo^{1.12}Re)^{-0.388} \quad \text{(viscous force dominant regime)} \tag{12}$$

$$E = (1 + 0.62We^{0.376})^{-1} \quad \text{(surface tension-inertial force dominant regime)} \tag{13}$$

4. Calculate Sr for given ω.

For $-5.5 \leq \log M \leq -3.9$, the agreements between the lift curves predicted by the ANN and the data are fairly well. Although the trend of the curve at $\log M = -3.2$ is not good for $Re < 0.2$, the trend at larger Re is acceptable. Even though there is no data for $Re < 5.7$ at $\log M = -6.6$, the ANN correlation reproduces the trend of C_L, i.e. the increase in Re largely decreases C_L. At $\log M = -10.6$, the predictions are reasonable for $Re > 600$; however at lower Re, at which no experimental data are available for training, the lift curve shows an un-physical trend.

Thus, the present ANN is capable to accurately predict C_L for a wide range of the relevant dimensionless groups. It however requires more data to avoid causing large errors in some parameter ranges, where no data are available.

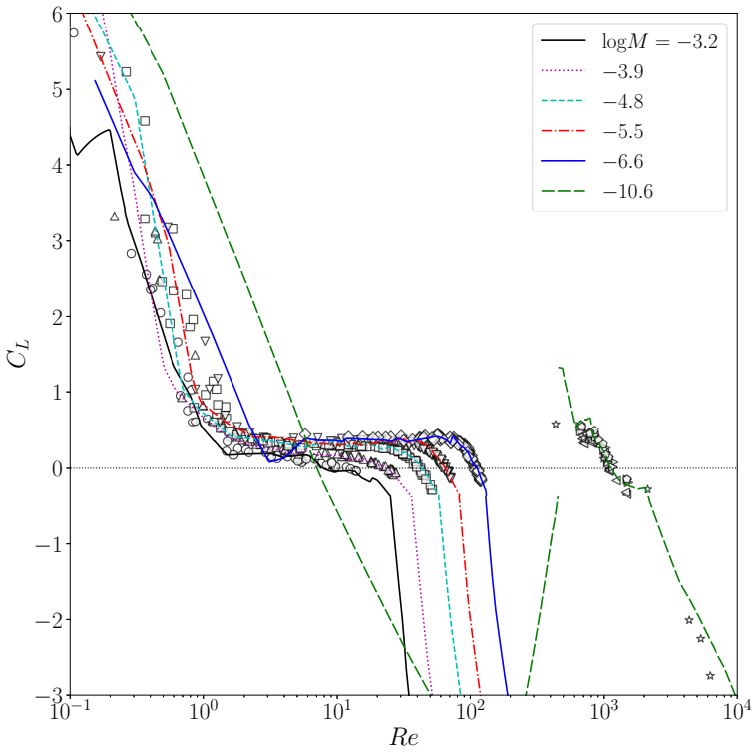

FIG. 8: Lift curves drawn using trained ANN model of $N_l = 3$ and $N_n = 10$. The shape correlations Eqs. (12) and (13) are used for E. The legends of the symbols are the same as those in Fig. 6. The shear rate, ω, used are 3.2 and 2.3 s^{-1} for $\log M \geq -6.6$ and $\log M = -10.6$, respectively.

3.3 Data Extension Using Available Model

As discussed in the previous section, the present ANN correlation gives relatively large errors at low Re ($\log M = -3.2, -6.6$) and intermediate Re ($\log M = -10.6$). Under these conditions, the bubble shape can be assumed to be almost spherical, and for spherical bubbles the following well-accepted semi-analytical correlation is available (Legendre and Magnaudet, 1998):

$$C_L^S = ([C_L^{SL}]^2 + [C_L^{SH}]^2)^{1/2} \tag{14}$$

where the lift coefficients of a low Reynolds number bubble, C_L^{SL} (Legendre and Magnaudet, 1997), and a high Reynolds number bubble, C_L^{SH}, are given by

$$C_L^{SL} = \frac{6}{\pi^2} \frac{2.255}{\sqrt{SrRe}\,[1 + 0.2Re/Sr]^{3/2}} \tag{15}$$

$$C_L^{SH} = \frac{1}{2}\left(\frac{1 + 16/Re}{1 + 29/Re}\right) \tag{16}$$

This correlation can provide some C_L data to cover the Re ranges of inaccurate predictions. It would be worth verifying a possibility of improving the accuracy of the present ANN model by re-learning with additional data.

Let us first examine whether the present ANN structure is capable of expressing Eq. (14) or not. The number of the data generated for this purpose is 400. The bubble Reynolds numbers and the dimensionless shear rate for the input are randomly selected. The Eötvös numbers are determined using the following drag correlation for spherical bubbles (Mei et al., 1994):

$$C_D = \frac{16}{Re}\left[1 + \left(\frac{8}{Re} + \frac{1}{2}\left(1 + \frac{3.315}{\sqrt{Re}}\right)\right)^{-1}\right] \tag{17}$$

Figure 9 shows comparisons between the generated data and predictions using the ANN correlation, which was trained with all the data up to 50,000 epochs. The data for low Re show some scatter because of the effects of Sr. The predictions agree well with the data in the whole range, and therefore, the effects of Re and Sr on C_L in Eq. (14) can be expressed well with the ANN correlation. Hence, the present ANN structure is expected to be able to correlate simultaneously the experimental data and additional data using Eq. (14).

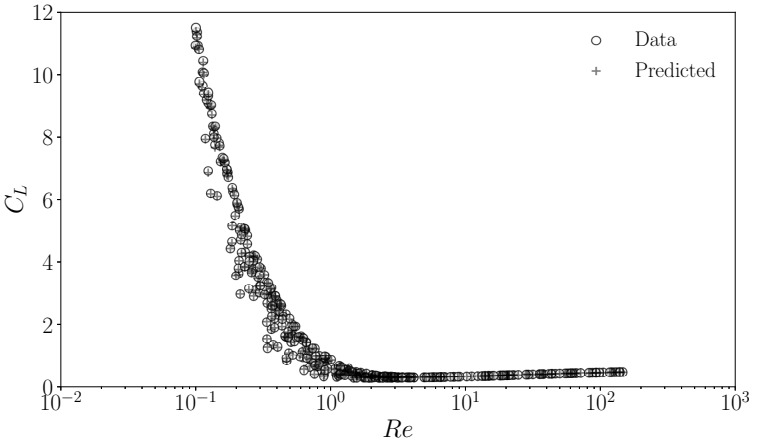

FIG. 9: Data created using the Legendre-Magnaudet correlation, Eq. (14), (circles) and predictions with ANN correlation ($N_l = 3$ and $N_n = 10$) (+ symbols).

The number of data added to the training set is 17 and the ranges of Re and Sr are shown in Table 4 (the upper three rows in the table). Only two data points of low Re are added in the data of $\log M = -3.2$. On the other hand, we add 15 data points in the low M data ($\log M = -6.6$ and -10.6) to supplement the database for a much wider Re range. Some data are also added in the intermediate Re ranges of $-6.6 \leq \log M \leq -3.2$ to maintain the decreasing trend of the lift curves by the ANN model as shown in Fig. 8.

Figure 10 shows comparisons between the training data and C_L predicted with the re-trained ANN model and lift curves drawn with the model. The predictions agree well with the training data and the characteristics of the lift curves become more reasonable than the previous predictions (Fig. 8) even with the small number of the additional data. The lift curve for $\log M = -10.6$ seems discontinuous at $Re \sim 460$, at which the shape correlation switches between Eqs. (12) and (13). Even though there are still no training data for $150 < Re < 440$, the trend of the lift curve is acceptable.

TABLE 4: Ranges of Re and Sr in training data added using Eq. (14) (upper three rows) and trained ANN model (lower five rows).

M	Re	Sr	Num. of data points
-3.2	$0.1 \sim 0.3$	$0.20 \sim 0.40$	2
-6.6	$0.1 \sim 4$	$0.03 \sim 0.06$	5
-10.6	$0.1 \sim 150$	$0.02 \sim 0.06$	10
-3.2	$27 \sim 46$	$0.12 \sim 0.22$	5
-3.9	$39 \sim 68$	$0.10 \sim 0.21$	5
-4.8	$62 \sim 113$	$0.084 \sim 0.20$	5
-5.5	$89 \sim 167$	$0.074 \sim 0.20$	5
-6.6	$139 \sim 304$	$0.054 \sim 0.20$	5

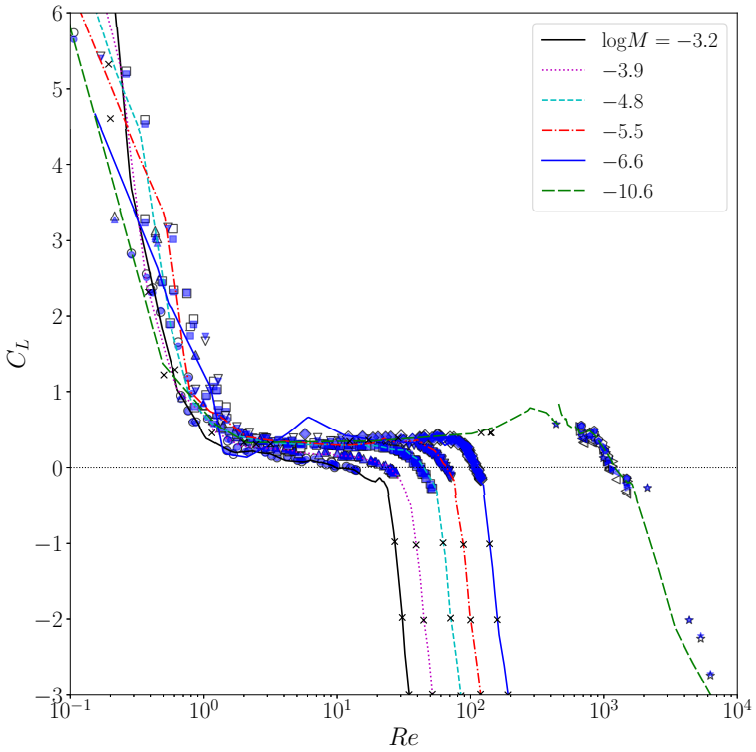

FIG. 10: Lift curves drawn using re-trained ANN model. Closed symbols: predicted; Open symbols: training data. Cross symbols: additional data.

3.4 Test Phase

The generalization performance of the trained ANN correlation is examined by predicting C_L of the test data. As shown in Fig. 11, the agreements between the predictions and the test data are fairly well. The characteristics of C_L are reproduced, i.e. C_L decreases with increasing Re at low Re, the decreasing rate mitigates, and then, C_L drops down to the negative lift regime. The errors in the predictions are shown in Fig. 12. Most data are within $\pm 10\%$ errors although some data

have relatively larger errors. The developed ANN correlation, thus, does not show remarkable overfitting and has a good generalization performance at least in the parameter ranges tested.

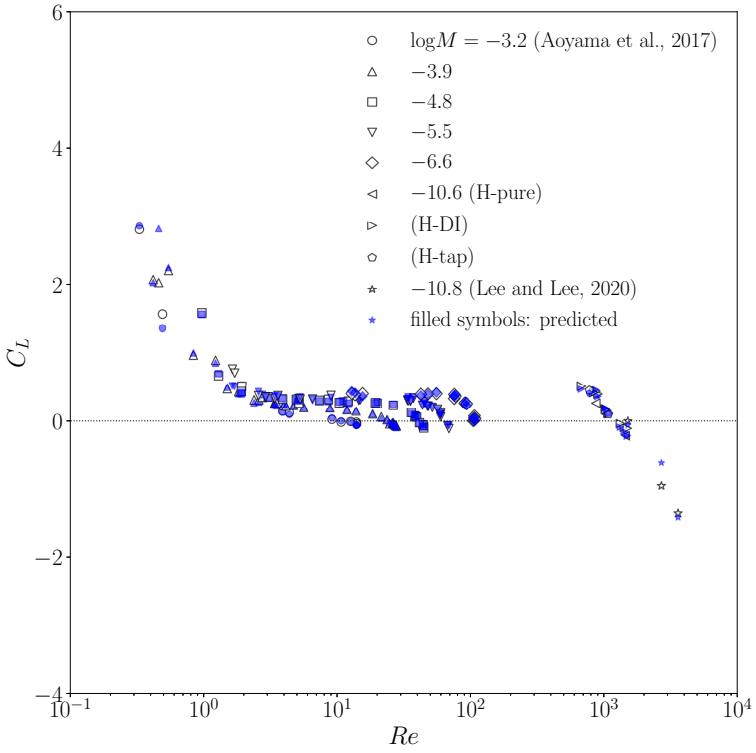

FIG. 11: Comparison between predicted C_L with test data ($N_l = 3$ and $N_n = 10$). Closed symbols: predicted; Open symbols: test data.

4. CONCLUSION

The characteristics of lift coefficients, C_L, of deformed bubbles in linear shear flows were well expressed by the artificial neural network trained with experimental databases available in literature. The K-folds cross validation was used to determine the numbers, N_l and N_n, of the hidden layers and the neurons, and $N_l = 3$ and $N_n = 10$ were selected based on the validation results. The predictions of the C_L agree well with the training data. Comparisons with the test data showed that the developed ANN correlation has a good generalization performance.

The ANN correlation with the simple fully-connected network was thus confirmed to be capable of expressing C_L well, and the applicable range covers both viscous force dominant and surface tension-inertial force dominant regimes. The main advantage of the ANN correlation is that the model can be easily improved by adding new lift data.

The simple ANN structure was selected from a point of view of computational costs in bubbly flow simulations. If a C_L-data table is prepared using the ANN and C_L is obtained from the table in bubbly flow simulations, a more complex structure can be selected for better accuracy. However, overfitting tends to take place for complex structures, and therefore, remedies for

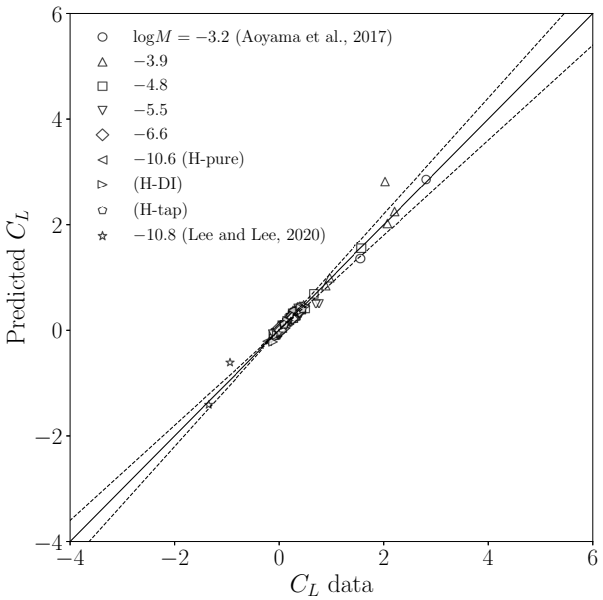

FIG. 12: Estimation errors for test data. $N_l = 3$ and $N_n = 10$. Dashed lines: $\pm 10\%$ errors.

overfitting, e.g. dropout, should be implemented.

In this study, the bubble Reynolds number Re, the Eötvös number Eo, the dimensionless shear rate Sr and the bubble aspect ratio E were used as the input features. It is also possible to develop ANN correlations to evaluate Re, Sr and E for given fluid properties, bubble size and liquid velocity.

ACKNOWLEDGMENTS

K. Hayashi and A. Tomiyama would like to express their thanks to financial supports by JSPS KAKENHI, Grant No. 20K04267 and 18H03756.

REFERENCES

Adoua, R., Legendre, D., and Magnaudet, J., Reversal of the lift force on an oblate bubble in a weakly viscous linear shear flow, *Journal of Fluid Mechanics*, vol. **628**, pp. 23–41, 2009.

Aoyama, S., Hayashi, K., Hosokawa, S., Lucas, D., and Tomiyama, A., Lift force acting on single bubbles in linear shear flows, *International Journal of Multiphase Flow*, vol. **96**, pp. 113–122, 2017.

Aoyama, S., Hayashi, K., Hosokawa, S., and Tomiyama, A., Shapes of ellipsoidal bubbles in infinite stagnant liquids, *International Journal of Multiphase Flow*, vol. **79**, pp. 23–30, 2016.

Beale, R. and Jackson, T., *Neural Computing: An Introduction*, IOP Publishing, New York, 1990.

Behkish, A., Hydrodynamics and mass transfer parameters in large-scale slurry bubble column reactors, PhD thesis, University of Pittsburgh, 2004.

Behkish, A., Lemoine, R., Sehabiague, L., Oukaci, R., and Morsi, B.I., Prediction of the gas holdup in industrial-scale bubble columns and slurry bubble column reactors using back-propagation neural networks, *International Journal of Chemical Reactor Engineering*, vol. **3**, 2005.

Chen, J., Hayashi, K., Hosokawa, S., and Tomiyama, A., Drag correlations of ellipsoidal bubbles in clean and fully-contaminated systems, *Multiphase Science and Technology*, vol. **31(3)**, pp. 215–234, 2019.

Enoki, K., Sei, Y., Okawa, T., and Saito, K., Prediction for flow boiling heat transfer in small diameter tube using deep learning (in Japanese), *Japanese Journal of Multiphase Flow*, vol. **31(4)**, pp. 412–421, 2017.

Hayashi, K., Hessenkemper, H., Lucas, D., Legendre, D., and Tomiyama, A., Scaling of lift reversal of deformed bubbles in air-water systems, *International Journal of Multiphase Flow*, vol. **142**, p. 103653, 2021.

Hayashi, K., Legendre, D., and Tomiyama, A., Lift coefficients of clean ellipsoidal bubbles in linear shear flows, *International Journal of Multiphase Flow*, vol. **129**, p. 103350, 2020.

He, K., Zhang, X., Ren, S., and Sun, J., Delving deep into rectifiers: Surpassing human-level performance on imagenet classification, *2015 IEEE International Conference on Computer Vision (ICCV)*, Santiago, Chile, 2015.

Hessenkemper, H., Ziegenhein, T., Lucas, D., and Tomiyama, A., Lift force coefficient of ellipsoidal single bubbles in water, *International Journal of Multiphase Flow*, vol. **138**, p. 103587, 2021.

Ioffe, S. and Szegedy, C., Batch normalization: Accelerating deep network training by reducing internal covariate shift, *Proceedings of the 32nd International Conference on Machine Learning*, Bach, F. and Blei, D. (Eds.), Vol. 37 of *Proceedings of Machine Learning Research*, PMLR, Lille, France, pp. 448–456, 2015.

Lee, W. and Lee, J.Y., Experiment and modeling of lift force acting on single high Reynolds number bubbles rising in linear shear flow, *Experimental Thermal and Fluids Science*, vol. **115**, p. 110085, 2020.

Legendre, D. and Magnaudet, J., A note on the lift force on a spherical bubble or drop in a low-Reynolds-number shear flow, *Physics of Fluids*, vol. **9**, pp. 3572–3574, 1997.

Legendre, D. and Magnaudet, J., The lift force on a spherical bubble in a viscous linear shear flow, *Journal of Fluid Mechanics*, vol. **368**, pp. 81–126, 1998.

Liu, L. and Bai, B., Flow regime identification of swirling gas-liquid flow with image processing technique and neural networks, *Chemical Engineering Science*, vol. **199**, pp. 588–601, 2019.

Maas, A.L., Hannun, A.Y., and Ng, A.Y., Rectifier nonlinearities improve neural network acoustic models, *Proceedings of ICML*, 2013.

Mei, R., Klausner, J., and Lawrence, C., A note on the history force on a spherical bubble at finite Reynolds number, *Physics of Fluids*, vol. **6**, pp. 418–420, 1994.

Mendelson, H.D., The prediction of bubble terminal velocities from wave theory, *International Journal of Multiphase Flow*, vol. **13(2)**, pp. 250–253, 1967.

Nesterov, Y., A method for unconstrained convex minimization problem with the rate of convergence $O(1/k^2)$, *Dokl. Akad. Nauk SSSR*, vol. **269(3)**, pp. 543–547, 1983.

Shibata, N., Miwa, S., Sawa, K., Takahashi, M., Murayama, T., and Tenma, N., Identification of upward two-phase flow regime transition region under high-pressure condition using deep learning, *Japanese Journal of Multiphase Flow*, vol. **35(1)**, pp. 93–100, 2021.

Tanaka, K., Prayitno, Y.A.K., Sejati, P.A., Kawashima, D., and Takei, M., Void fraction estimation in vertical gas-liquid flow by plural long short-term memory with sparse model implemented in multiple current-voltage system (pLSTM-SM-MCV), *Multiphase Science and Technology*, 2022.

Tanaka, M., Study on practical numerical methods for multiphase multicomponent thermo-hydrodynamic fields, PhD thesis, Kobe University, 2010.

Tanaka, M., Hayashi, K., and Tomiyama, A., An evolving numerical method for designing slurry bubble column reactors, *Kagaku-Kogaku Ronbunshu*, vol. **31(1)**, pp. 17–24, 2010.

Tomiyama, A., Kataoka, I., Zun, I., and Sakaguchi, T., Drag coefficients of single bubbles under normal and micro gravity conditions, *JSME International Journal Ser. B: Fluids and Thermal Engineering*,

vol. **41(2)**, pp. 472–479, 1998.

Tomiyama, A., Tamai, H., Žun, I., and Hosokawa, S., Transverse migration of single bubbles in simple shear flows, *Chemical Engineering Science*, vol. **57**, pp. 1849–1858, 2002.

Weiner, A., Hillenbrand, D., Marschall, H., and Bothe, D., Data-driven subgrid-scale modeling for convection-dominated concentration boundary layers, *Chemical Engineering & Technology*, vol. **42**, pp. 1349–1356, 2019.

Ziegenhein, T., Tomiyama, A., and Lucas, D., A new measuring concept to determine the lift force for distorted bubbles in low Morton number system: Results for air/water, *International Journal of Multiphase Flow*, vol. **108**, pp. 11–24, 2018.